Surface-core-level-shift low-energy photoelectron diffraction: The 2×1-Si(001) surface

R. Gunnella
Unitá INFM-Dipartimento di Matematica e Fisica, Università di Camerino, Via Madonna delle Carceri, 62032 Camerino (MC), Italy

E. L. Bullock and L. Patthey
Insitut de Physique Expérimentale, Université de Lausanne, CH-1015 Lausanne-Dorigny, Switzerland

C. R. Natoli
INFN, Laboratori Nazionali di Frascati-Casella Postale 13, 00044 Frascati, Italy

T. Abukawa and S. Kono
Laboratory of Surface Physics, Research Institute for Scientific Measurements, Tohoku University, Sendai 980-77, Japan

L. S. O. Johansson*
Department of Synchrotron Radiation Research, Institute of Physics, Lund University, Box 118, S-221 00 Lund, Sweden
(Received 7 August 1997)

Surface-core-level-shift photoelectron diffraction at the surface-sensitive kinetic energy of the photoelectron has been used as a powerful method for the determination of the clean surface structure of 2×1-Si(001). With the aid of a theoretical interpretation based on full multiple scattering with complex potential, we show that an extreme sensitivity to the short-range order due to the chosen photoelectron kinetic energy range can be achieved. As a consequence results obtained are shown exempt from spurious effects due to the partial order on the surface, which could be detrimental to other conventional diffraction techniques for structures determination. The photoelectron diffraction experiment was performed at room temperature and the low-energy electron diffraction showed a 2×1 single domain pattern with diffuse lines due to higher-order reconstructions. In the analysis different reconstructions [$p(2\times1)$, $p(2\times2)$, and $c(4\times2)$] were considered to check the stability of the optimization structural parameters during the automatic search procedure for the best fit. The structural parameters derived by such an analysis were compared with several recent total-energy calculations performed for the three reconstruction geometries taken into consideration. [S0163-1829(98)02223-1]

I. INTRODUCTION

A quite formidable problem is represented by the study of clean surfaces. In many surface structure techniques a significant problem is to reduce the overwhelming contribution from the bulk in order to attain more detailed insight of the surface structural properties.

On the other side, scanning microscopies necessarily disregard the interaction between the very first layer (the interface with the vacuum) and the atoms underneath, which is responsible of most surface properties. Moreover some difficulties arise from the interplay between structural and electronic features during imaging of surface states.

The present technique turns out to be quite peculiar because of the isotropic nature of the emitted low kinetic energy electrons. This characteristic allows surface-core-level-shift low-energy photoelectron diffraction (SCLS-PD) to evenly probe the atomic structure around the photoemitter, and to resolve by a single experiment the three-dimensional geometry of the surface under study by monitoring the angular anisotropy of the photoemission peak originating from surface shifted core levels.

Quite recently, Gota *et al.*[1] and Bullock *et al.*[2] have shown the degree of sensitivity of such a technique. In this work we shall report the method used in obtaining the results above quoted. In particular the application to the case of the 2×1-Si(001) surface,[2] as a prototypical case, deserves an extended description of the results obtained. Furthermore, to our knowledge, only very few experiments are currently capable of giving a realistic description of such a surface, in reasonable agreement with the massive amount of theoretical calculations available. The main reason for this lack of agreement is certainly related to some degree of disorder observed on several semiconductor surfaces, which creates some difficulties to diffraction techniques such as low-energy electron diffraction (LEED) or surface x-ray diffraction because of their extended coherence length.

From the structural point of view, the present technique is similar to LEED, but the signal carrying information (the photoemission intensity) can be optimized because of the absence of interference effects coming from the scattering processes that originate at different planes in the bulk. With the help of the high-resolution photoemission, now fully available at third generation synchrotron radiation sources, the effect of the surface potential that induces an energy shift to the core-level photoemission peak of those atoms that are directly involved in the surface termination, allows in principle the capability to sort out, among the several contributions to the photoemission, those coming from the atoms of interest.

Actually there are two kinds of obstacles to this kind of study. First, on many surfaces the SCLS's are small com-

pared to both the intrinsic linewidth of the core levels and the instrumental broadening. This is particularly true for many metals in which the surface structure and thus the chemical environment is not very different from the bulk. Indeed, the very existence and number of SCLS's is often a cause of debate due to these limitations. The second obstacle is the question of the structural origins of the observed SCLS's. In a previous Letter[2] we showed that SCLS-PD could be used to assign the structural origin of the SCLS peak under study by comparison of the experimental angular anisotropy in the photoemission intensity with multiple scattering calculations of the angular resolved photoemission cross section. The assignment of the Si $2p$ core level shifted by 0.5 eV towards higher kinetic energy on the 2×1-(001) surface was shown unambiguously to originate from the up atom of a highly ionic dimer.

The problem of ionicity of the dimer bond is also related to the nature of the local reconstruction, because no realistic model exists that can explain the LEED quarter order spots without asymmetric dimers. In fact Ihm *et al.*[3] demonstrated that the room-temperature (RT) 2×1 reconstruction observed by LEED is not the ground state of the clean Si(001) surface, but several higher-order reconstructions occur with lower total energy, and suggested the existence of an order-disorder phase transition for the disappearance of the higher-order diffraction spots. This phase transition was observed at about 200 K from the $c(4\times2)$ to the 2×1 by Tabata *et al.*[4]

Scanning tunneling microscopy (STM) topographs of the Si(001) surface taken at room temperature revealed a surface consisting of approximately an equal number of buckled and unbuckled dimers as well as region of (2×1), $p(2\times2)$, and $c(4\times2)$ symmetries, and a relatively large number of defects.[5,6] The authors did not rule out the possibility that the appearence of nonbuckled dimers could be due to dynamic buckling on a time scale that is short compared to the STM measurement time. Indeed, more recent low-temperature STM measurements showed that upon cooling to 120 K, the number of buckled dimers increases together with the extent of higher-order reconstructions domains.[6]

In the present paper we shall discuss in detail the structural model of Si(001) putting emphasis on the sensitivity of the present technique to the structural analysis of solid clean surfaces. Even if a reduced set of experimental data is reported, we are going to demonstrate the stability of the structural results obtained by comparison with fully converged multiple scattering calculations. We face the problem of the Si(001)-2×1 surface at RT, where several reconstruction domains are supposed to coexist by looking at the effects of a single reconstruction on the structural parameters. What we measured is a PD signal that corresponds to the time-averaged dimer structure of this disordered surface that we expect to be close to a $c(4\times2)$ or a $p(2\times2)$ reconstruction.

The room-temperature experiment on the 2×1-Si(001) surface as characterized by LEED introduces also the problem of the short-range order character of SCLS-PD when compared with LEED. The latter, because of its large coherence length, shows a diffuse intensity due to the different reconstruction domains on the surface, while the former technique is more sensitive to the real geometry of atoms surrounding the photoemitter. A similar behavior versus LEED observations has been reported in valence-band photoemission.[7]

The present paper will include in Sec. II the theoretical background of the method used. For the experimental description we refer to the work of Bullock *et al.*[2] The fitting procedure will be reported in Sec. III, while discussion and conclusion will follow in Sec. IV.

II. THEORY

We calculate the cross section for the photoemission of a core electron from a system containing N electrons along the direction $\vec{k}_\beta$ with energy $k_\beta^2=\omega-I_c-\Delta E_\beta$ where ω is the energy of the impinging photon, I_c is the core ionization potential and ΔE_β is the excitation energy left into the system. We shall use throughout atomic units for lengths and Rydberg units for energies.

The problem in its generality has been dealt with in Ref. 8. The computer code will be described elsewhere.[9] We shall only recall here the main formulas of Ref. 8, referring to that paper for notations and more complete discussion of the underlying physics. There it was shown that the cross section in question can be written as

$$\frac{d\sigma}{d\hat{k}_\beta}=8\pi^2\alpha\omega\sum_{m_0}\left|\left(\sum_\alpha S_\alpha f_\alpha^-(\vec{r};\vec{k}_\beta)|\hat{\epsilon}\cdot\vec{r}|\phi_{l_0m_0}^c(\vec{r})\right)\right|^2\rho(k_\beta^2), \tag{1}$$

where $\hat{\epsilon}$ is the photon polarization vector, α is the fine-structure constant, $\rho(k_\beta^2)=k_\beta/(16\pi^3)$ is the final state density for the outgoing plane wave with wave number k_β, S_α is the overlap integral of the ''passive'' electrons given by $\langle\tilde{\Psi}_\alpha^{N-1}|\Psi_G^{N-1}\rangle$, $\phi_{l_0m_0}^c(\vec{r})$ is the core electron wave function with angular momentum $L_0\equiv(l_0,m_0)$ and $f_\alpha^-(\vec{r};\vec{k}_\beta)$ is the time-reversed scattering wave function for the photelectron in channel α with energy $k_\alpha^2=\omega-I_c-\Delta E_\alpha$ obeying the system of coupled Schrödinger equations

$$(\Delta+k_\alpha^2)f_\alpha^-(\vec{r};\vec{k}_\beta)=\sum_{\alpha'}V_{\alpha\alpha'}(\vec{r})f_{\alpha'}^-(\vec{r};\vec{k}_\beta) \tag{2}$$

with interchannel potentials $V_{\alpha\alpha'}(\vec{r})$ and asymptotic boundary conditions

$$f_\alpha^-(\vec{r};\vec{k}_\beta)\approx e^{i\vec{k}_\beta\cdot\vec{r}}\delta_{\alpha\beta}+f_\alpha^-(k_\alpha\hat{r};\vec{k}_\beta)\frac{e^{-ik_\alpha r}}{r}. \tag{3}$$

In Eq. (1) an extra factor of 2 takes into account the spin degrees of freedom, which will be henceforth neglected.

In principle it is certainly possible to solve the set of coupled equations (2) only in terms of the channel β of interest, obtaining each $f_\alpha^-(\vec{r};\vec{k}_\beta)$ as a function of $f_\beta^-(\vec{r};\vec{k}_\beta)$. This elimination process leads to an effective Schrödinger equation for the channel in question with a complex optical potential $V_{\rm eff}^\beta(\omega,\vec{r})$ that describes the effect of the eliminated channels

$$[\Delta+k_\beta^2-V_{\rm eff}^\beta(\omega,\vec{r})]f_\beta^-(\vec{r};\vec{k}_\beta)=0. \tag{4}$$

Substitution into Eq. (1) yields for the cross section

$$\frac{d\sigma}{d\hat{k}_\beta}=8\pi^2\alpha\omega\sum_{m_0}|[S_{\rm op}^{\beta}(\omega)f_\beta^-(\vec{r};\vec{k}_\beta)|\hat{\epsilon}\cdot\vec{r}|\phi_{l_0m_0}^c(\vec{r})]|^2\rho(k_\beta^2),$$

where $S_{\rm op}^{\beta}(\omega)$ is a complicated nonlocal operator acting on $f_\beta^-(\vec{r};\vec{k}_\beta)$ as

$$\int d^3r' S_\beta(\omega;\vec{r},\vec{r}')f_\beta^-(\vec{r}';\vec{k}_\beta).$$

In the following we shall make the *ansatz* of locality and write instead

$$S_\beta(\omega;\vec{r})f_\beta^-(\vec{r};\vec{k}_\beta)\approx S_\beta(\omega)f_\beta^-(\vec{r};\vec{k}_\beta),$$

the last step being a consequence of the excitation process. Notice that $S_{\rm op}^{\beta}(\omega)$ does not carry any dependence on the direction of $\vec{k}_\beta$ since it can be expressed only in terms of the inverse of the operators $(\Delta+k_\alpha^2)$.

The reduction process sketched above is equally valid for the completely relaxed channel ($\Delta E_0=0$), which henceforth will be labeled by $\beta=0$, and for electrons that have experienced some energy loss ($\Delta E_\beta\neq 0$), like those undergoing plasmon losses. It is worth noticing that apart from the effective optical potential, on which we shall comment briefly, the structural basis for the diffraction mechanism is the same for both types of electrons. We are led therefore to the following expression for the photoemission cross section:

$$\frac{d\sigma}{d\hat{k}_\beta}=8\pi^2\alpha\omega|S_\beta(\omega)|^2\times\sum_{m_0}|[f_\beta^-(\vec{r};\vec{k}_\beta)|\hat{\epsilon}\cdot\vec{r}|\phi_{l_0m_0}^c(\vec{r})]|^2\rho(k_\beta^2). \quad (5)$$

Considerations similar to those developed in Ref. 10 lead us to identify the non-Coulombic part of $V_{\rm eff}^{\beta}(\omega,\vec{r})$ with the self-energy of a uniform interacting electron gas with density given by the local density of the system under study and in the plasmon pole approximation for the dielectric function to the Hedin-Lundqvist (HL) potential.[11] In this approximation we can assume that the effective potential is roughly the same for the elastic and the inelastic channels since the corresponding total charge densities of the system in these configurations are expected to be very similar.

As a result of all this we are then left with the problem of the solution of Eq. (4) with boundary conditions (3). This is a scattering problem with complex potential. In the following when not necessary we shall drop the channel index β from $S_\beta(\omega)$ and the wave function $f_\beta^-(\vec{r};\vec{k}_\beta)$ considering the scattering wave function $f^+(\vec{r};\vec{k})=[f^-(\vec{r};\vec{k})]^*$.

In the muffin-tin approximation the charge density of the system, the potential and the solution of the related SE are represented piecewise according to the partitioning of the space into region I, the space enclosed by spheres I_i of radius ρ_i around each atomic position $\vec{R}_i$, and region II, the space outside the atomic spheres called the interstitial region and extending to infinity due to the absence of an outer sphere, which is unsuitable when dealing with surfaces. We shall neglect the outer sphere region and represent the surface potential by a potential step joining the muffin-tin negative interstitial constant potential with the zero potential region of the vacuum outside the system. Inside the muffin-tin sphere I_i one can represent the scattering wave function, which is a function of $\vec{r}_i=\vec{r}-\vec{R}_i$, as

$$f^+(\vec{r}_i;\vec{k})=\sum_{LL'}4\pi i^l Y_L(\hat{k})B_{L'}^i(L)\underline{R}_{l'}^i(r_i)Y_{L'}(\hat{r}_i) \quad (6)$$

using throughout real spherical harmonics.

Here the function $\underline{R}_{l'}^i(r_i)$ is normalized so that

$$\underline{R}_l^i(r_i)=\frac{R_l^i(r_i)}{k\rho_i^2 W[j_l(r_i)R_l^i(r_i)]_{\rho_i}},$$

where $j_l(r)$ is the usual Bessel function, $W[f,g]_\rho=(fg'-gf')|_\rho$ is the Wronskian of the two functions $f(r)$ and $g(r)$ calculated at $r=\rho$, and $R_l^i(r_i)$ is the regular solution of the radial SE inside sphere I_i with angular momentum l behaving at the origin as r_i^l.

With this normalization it is possible to show[8,10] that the quantities $B_{L'}^i(L)$ in Eq. (6) controlling the amplitude of each partial wave inside sphere I_i are the same quantities that control the amplitude of the spherical waves in the asymptotic region emanating from the same sphere. In fact in this latter region, and also in region II due to the absence of the outer sphere, one can write, indicating by $h_l^+(r)$ the outgoing spherical Hankel function of order l,

$$f^+(\vec{r}_i;\vec{k})=\sum_L 4\pi i^l Y_L(\hat{k})\Big[j_l(kr)Y_L(\hat{r})-i\sum_{j,L'}B_{L'}^j(L)h_{l'}^+(kr_j)Y_{L'}(\widehat{r_j})\Big]. \quad (7)$$

From Eqs. (6) and (7) it is clear that the quantities $B_{L'}^i(L)$ are to be interpreted as total scattering amplitudes in channel L' for all waves incident on the atom located at site i coming from everywhere in the system in response to an exciting wave in channel L.

They therefore satisfy a set of compatibility equations called the MS equations

$$B_{L'}^i(L)=-t_{l'}^i J_{L'L}^{io}-t_{l'}^i\sum_{j\neq i}\sum_{L''}G_{L'L''}^{ij}B_{L''}^j(L) \quad (8)$$

or in the more usual form

$$\sum_{jL''}[(T_a^{-1})_{L'L''}^{ij}+G_{L'L''}^{ij}]B_{L''}^j(L)=-J_{L'L}^{i0}, \quad (9)$$

where we have defined the matrix $(T_a^{-1})_{L'L''}^{ij}=(1/t_{l'}^i)\delta_{ij}\delta_{L'L''}$. Here t_l^i is the atomic t matrix of the atom at site i given by

$$t_{l'}^i=i\frac{W[j_{l'}(kr_i),R_{l'}^i(r_i)]_{\rho_i}}{W[h_{l'}^+(kr_i),R_{l'}^i(r_i)]_{\rho_i}}=e^{i\delta_l^i}\sin(\delta_l^i),$$

δ_l^i being the lth phase shift of the potential inside sphere I_i, and $G_{LL'}^{ij}$ is the amplitude of propagation from site j to site i

of a free spherical wave of angular momentum L around site i and L' around site j given by

$$G^{ij}_{LL'} = 4\pi \sum_{L''} i^{l+l''-l'} C^{L''}_{LL'} [-ih^{+}_{l''}(kR_{ij})] Y_{L''}(\hat{R}_{ij}) = N^{ij}_{LL'} - iJ^{ij}_{LL'} \quad (10)$$

the last equation following from the relation $-ih^{+}_{l}(r) = n_l(r) - ij_l(r)$ with the obvious definition of $N^{ij}_{LL'}$ and $J^{ij}_{LL'}$. In this last equation $\vec{R}_{ij} = \vec{R}_i - \vec{R}_j$ and

$$C^{L''}_{LL'} = \int Y_L(\hat{r}) Y_{L'}(\hat{r}) Y_{L''}(\hat{r}) d\hat{r}$$

are the Gaunt coefficients. Finally the factor $J^{io}_{L'L}$ on the right-hand side of Eq. (8) is the amplitude of the exciting spherical wave of angular momentum L around the origin as seen from site i and is given by Eq. (10).

Equation (8) states the fact that the total scattering amplitude $B^{i}_{L'}(L)$ at site i is given by the sum of the atomic scattering amplitude at the same site times the exciting amplitude plus the amplitude of all the waves that come from all other sites with any angular momentum, propagate to site i, and are scattered by the atom located there.

Due to the localization of the initial core state, which we shall suppose to be located at site o (the origin), we need only that part of the electron wave function inside sphere I_o. Therefore taking the complex conjugate of Eq. (6), written for site o and inserting it into Eq. (5) we obtain for the photoemission cross section

$$\frac{d\sigma}{d\hat{k}} = 8\pi^2 \alpha \omega \frac{k}{\pi} |S(\omega)|^2 \sum_{m_0} \left| \sum_{LL'} [M^{L_0}_{L'} B^{o}_{L'}(L)]^* i^{-l} Y_L(\hat{k}) \right|^2 \quad (11)$$

with

$$M^{L_0}_{L'} = \langle \underline{R}^{o}_{l'}(r) Y_{L'}(\hat{r}) | \hat{\epsilon} \cdot \vec{r} | \phi^{c}_{L_0}(\vec{r}) \rangle. \quad (12)$$

To proceed further we solve Eq. (9) for $B^{o}_{L'}(L)$ as

$$B^{o}_{L'}(L) = -\sum_{jL''} \tau^{oj}_{L'L''} J^{jo}_{L''L}, \quad (13)$$

where we have introduced the inverse of the multiple scattering matrix

$$\tau^{ij}_{LL'} = [(T_a^{-1} + G)^{-1}]^{ij}_{LL'} \quad (14)$$

known as the scattering path operator, which describes the total amplitude of propagation from one site to another in the angular momentum representation. Moreover using the relation[8]

$$\sum_{L} J^{jo}_{L'L} i^{l} Y_L(\hat{k}) = i^{l'} Y_{L'}(\hat{k}) e^{i\vec{k}\cdot\vec{R}_{jo}} \quad (15)$$

we finally obtain for the photoemission cross section from a core state

$$\frac{d\sigma}{d\hat{k}} = 8\pi^2 \alpha \omega \frac{k}{\pi} |S(\omega)|^2 \times \sum_{m_0} \left| \sum_{j} \sum_{LL'} M^{L_0}_{L} \tau^{oj}_{LL'} i^{l'} Y_{L'}(\hat{k}) e^{i\vec{k}\cdot\vec{R}_{jo}} \right|^2. \quad (16)$$

This latter form is very rewarding in that it can be read in terms of physical processes. It simply says that the cross section for emission of a photoelectron along $-\vec{k}$ is the result of an interference process in which all composite amplitudes of all possible events describing the creation of a photoelectron, its propagation through the system, and the final escape into the vacuum interfere to create the final total amplitude whose modulus square is proportional to the intensity of the photocurrent along $-\vec{k}$. These composite amplitudes are obtained as the product of the amplitude $M^{L_0}_{L}$ for the creation of the electron at site o in angular momentum L, times the amplitude of propagation $\tau^{oj}_{LL'}$ from site o to any other site j with final angular momentum L', times the amplitude $Y_{L'}(\hat{k})$ for emission along the direction $-\hat{k}$ as seen from site j, times the phase factor $e^{i\vec{k}\cdot\vec{R}_{jo}}$ that takes into account the phase relation of the electronic wave between sites o and j. This form of the cross section follows very closely the usual three-step model for the photoemission process.

Following the way shown by Tyson *et al.*,[10] we built the potential for the calculation superposing atomic charge density from tabulated self-consistent (SCF) atomic wave functions[12] following the Mattheis procedure.

After a suitable choice of the size of the atomic radii, which will be discussed in the following, we built the cluster charge density and Coulombic part of the muffin-tin potential after the spherical average of the superposed atomic potentials. The exchange and correlation (XC) part of the potential was instead obtained from the Hedin-Lunqvist potential.[11] It is known that its imaginary part reproduces quite well the electron mean free path in metals and semiconductors.[13] In the region outside the atomic spheres the Coulomb potential and charge were set equal to their volume averaged values. In this scheme the constant value of the charge was used to obtain the complex XC part of the interstitial constant potential.

The simplifying approximation of the full potential to a constant value in the interstitial region is certainly a crude one for a covalent solid. To check the sensitivity of the technique to a different method of construction of the potential we compared results obtained in the way outlined above with those obtained by using a SCF solution of the Si bulk potential in a linear muffin-tin orbital approximation,[14] using no regions of constant potential, and using, on the contrary, empty spheres of electronic charge in order to simulate the direction of the bond. Results following this second procedure turned out to be indistinguishable from the muffin-tin case. The calculation of the photoemission anisotropy was obtained after full inversion of the MS matrix, since for this cluster and at low photoelectron kinetic energies ($\approx$40 eV) the MS series does not converge.[10] Full advantage of the symmetry point group (C_s) was taken. Even with this low surface symmetry involving only a factor 2 of reduction of the MS matrix, calculation with clusters containing more

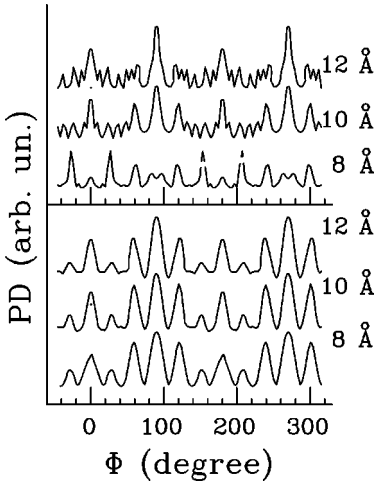

FIG. 1. In the bottom and top panel are reported the calculations of photoelectron diffraction (PD) azimuthal patterns respectively in the presence and absence of a complex potential, for a spherical cluster of Si of 8, 10, and 12 Å of radius. The kinetic energy is the same as that used in the present experiment. The convergence is observed when 10 Å cluster radius is used in complex potential mode calculation.

than 100 atoms can be done in a few minutes of CPU on Digital alpha-VAX machines per energy point.

The scattering from the surface potential was taken into account only via the usual refraction condition of the outgoing photoelectron through the potential step. Because of the low kinetic energy involved in the experiment some doubts could arise about the planarity of the barrier constituted by the interface with vacuum. In fact if photoelectrons were sensitive to the local structure of the interstitial potential the refraction law would not be valid. However, optimized values of the interstitial potential (5.5 eV) and the angle of propagation inside the solid (40°) were found consistent with the refraction law. Independent confirmations of these findings were obtained from other experiments done under the same experimental conditions on the As/Si(111) and As/Si(001) surfaces giving the same indications for the main parameters of the calculation.[15]

For a realistic description of the surface and bulk PD patterns it was found essential to calculate the PD scattering amplitude with an effective optical potential that incorporates the attenuation of the photoelectronic wave via complex atomic phase shifts and complex interstitial potential. The importance of the use of a built-in complex potential is briefly shown in Fig. 1 where calculations for azimuthal diffraction patterns for photoelectrons emitted from an ideal Si(001) surface are reported. As can be observed, the insertion of the complex potential is extremely useful in the region of energy used, in which the opening of channels due to the excitation of a single plasmon in the solid is crucial to describe the correct propagation of the photoelectron. Sizable differences and anisotropy features not detected in the experimental pattern are obtained if the complex part is mimicked by an exponential mean-free-path–based damping. Figure 1 clearly illustrates the difficulty of achieving convergence in the size of the cluster (8, 10, or 12 Å) when the complex part of the potential is set to zero (top panel), as compared with the case in which the complex potential is used (bottom panel). Moreover any convolution of the experimental data with some broadening function cannot be performed because of the angular experimental mode, while a multienergy (average on the peak width) contribution to the calculated pattern is ineffective in reducing the effects of the Fig. 1. In the present calculation with complex potential, convergence in the cluster size was obtained after including five planes of atoms with a cutoff radius of 10 Å around the photoabsorber corresponding to more than 100 atoms. This is the expected value, since it roughly corresponds to twice the photoelectron mean free path, i.e., the damping distance for the amplitude of propagation in Eq. (16), at the chosen kinetic energy ($\approx$40 eV). Due to the uncertainty with which we know the parameters of the potential, the minimization procedure involved also those details of the potential that can be questionable for the two main approximations used: the muffin-tin and the surface potential barrier. For this reason, during the automatic trial and error procedure that led to a minimization of an error function (R factor) the Coulombic part of the constant muffin-tin complex potential and the charge density (from which the XC potential is calculated) were also changed and continuously compared with value obtained from band-structure calculation of the surface.

III. ANALYSIS AND RESULTS

In a previous paper we described the measurement of the PD angular intensity of the Si $2p$ photoemission core level taking its origin at the up atom of the dimer and shifted 0.5 eV towards higher kinetic energy with respect to the bulk photoemission core level. By a fitting procedure the area of such a surface core-level peak is singled out from the contributions of Si atoms occupying other surface or bulk atomic sites.[2] Multiple scattering calculations of the angular photoemission cross section related to the selected position of the photoemitter atom on the surface are compared with the experimental curve after normalization and the error function minimized in order to obtain the structural parameters, i.e., position of atoms in the first, second, and third layers of the Si(001) bulk terminated surface, while deeper atoms are considered frozen in their bulk positions. Other parameters involved in the calculation are those connected to the muffin-tin potential, i.e., atomic radii, interstitial constant charge density, and potential. Furthermore we allowed small adjustments around the nominal values of the kinetic energy and the emission angle of the photoelectron inside the solid.

Each photoelectron diffraction pattern was calculated at a single kinetic energy point to be compared with the experimental intensity obtained from the area of the photoemission peak. The correctness of the procedure was verified with great accuracy comparing the experimental anisotropy of the area of the spin doublet with the maximum of the intensity of the major spin-orbit component (Si $2p_{3/2}$). In fact variation in the statistical ratio of the two spin-orbit components is less than 5% in the Si $2p$ core level and then neglected.

The value of the internal kinetic energy found by a minimization procedure was checked in agreement with the value of experimental photoemission kinetic energy and the experimental surface work function as measured after each experiment by means of the kinetic energy of the high energy tail of secondary electrons with the sample biased by -10 V.

Analysis of experimental curves was performed by using a Simplex[16] minimization procedure of the R-factor function of the parameters, defined as the absolute value of the differences between normalized theory and experiment, divided by the number of experimental points. In order to probe the largest possible parameter space a Metropolis algorithm[16] was implemented to simulate an annealing during the minimization procedure. This minimization, though slow, was efficient in the minimum search. At each iteration the main set of coordinates of the atoms of the dimer was changed and the full calculation redone. No tensor linear approximation was attempted. The influence due to different starting random points was checked to be well inside the error bars of the minimization. Each minimization, according to the different cases, made use of 600–800 different calculations. Local minima were avoided by means of a mesh with steps of 0.02 and 0.01 Å only in the very last phase of the procedure. The minimization was done for three different reconstructions $c(4\times2)$, $p(2\times2)$, and $p(2\times1)$, in order to check the stability of the final results. During the entire minimization procedure the majority-minority domain ratio was treated as a fitting parameter, leading to a striking predominance of the majority domain, i.e., dimer bond along the $[1\bar{1}0]$ direction, in the ratio $75\%\pm5\%$. At the start of the procedure for each reconstruction only the dimer atom positions were moved with different choices for the relaxation of the substrate atoms. For the best option of inner plane relaxation a minimization of all the atoms together was accomplished. Due to the nature of the localization of the probe to the very first plane, the sensitivity of the technique to the inner planes was found to be rather weak, even though it cannot be excluded that some scattering geometries could increase the importance to these structural parameters, for the present experimental conditions we did not observe any sensitivity (inside reasonable variations of the parameters around the nominal positions) to atoms beyond the third plane.

The error bars were determined with relation to the random noise, which affects the minimization. Changes in the theoretical input parameters, such as interstitial complex potential or muffin-tin radii, were used as random noise generators for the degree of uncertainty in the theory due to the tailoring of the muffin-tin model for the description of the potential. The error bars, obtained on the basis of perturbations induced in the best fit solution parameters by these random noise generators, were found to be well inside the errors obtained by looking at the whole set of representations of the surface geometry whose agreement with the experiment is considered satisfactory.

A χ^2 test was performed to evaluate the goodness of the fit. We estimated the total statistical error σ (theoretical errors due to theoretical model plus experimental errors) to be of the order of 7–8 %. With this value of the error we accepted as a good fit a value of 0.8–1 for the quantity $\sigma^2\chi^2$ for the 120 experimental points of the fit. This number is to be compared with a value of our R factor of 0.05–0.06 in the case of the $p(2\times2)$ and $c(4\times2)$ reconstruction, while a value of about 0.08 is obtained for the $p(2\times1)$ reconstruction. In comparison a bad fit obtained with $R=0.24$ would correspond to a value of $\sigma^2\chi^2$ of about 10, clearly off of any reasonable agreement with the experiment. We evaluated the errors of the fitting parameters by considering half the statistical spread of their values in case of acceptance of the fit for a R factor lower than 0.06. The test was also important to establish that, given the level of agreement, the single anisotropy photoelectron diffraction curve was statistically sufficient for the structural parameters' determination. In Fig. 2 are reported all the curves, which in fact are considered to have the highest observed level of goodness in the comparison with the experiment for the case of the $c(4\times2)$, $p(2\times2)$, and $p(2\times1)$.

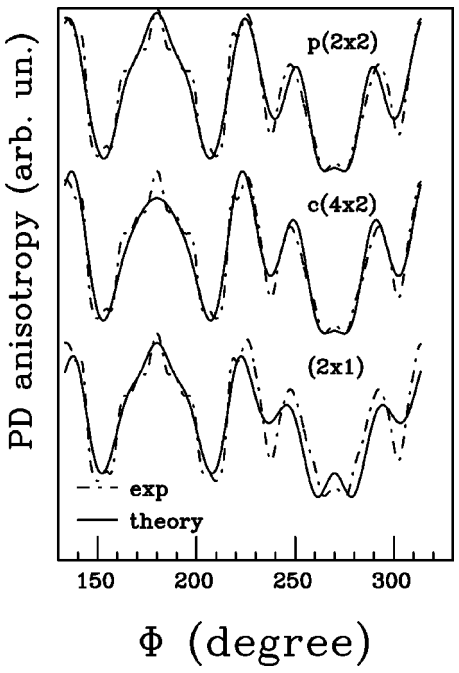

FIG. 2. Level of agreement of Si $2p$ PD azimuthal calculation for the three surface periodicities $p(2\times1)$, $c(4\times2)$, $p(2\times2)$ of the Si(001) surface when compared with experiment reported in dashed line. An experiment has been performed with a polar angle detection of 45° and a photon beam of 130 eV and angle of incidence 5° from the normal to the surface in the plane of the detection, on the same side of detected electron. The azimuthal angle 180° corresponds to majority domain row direction [110]. The dimer bond is along the direction $[1\bar{1}0]$ (270°).

Among the parameters, a high degree of correlation exists for the complex interstitial potential and the emission angle. The real part of the interstitial potential was found to be $5.5(\pm0.5)$ eV, the emission angle about $40°(\pm0.5°)$, the calculated mean free path 5 Å, and the interstitial charge density $0.006(\pm0.001)$ electron/(a.u.)^3

Furthermore the degree of overlapping of MT spheres was chosen to vary between 5 and 10 % providing a sizable improvement when compared with the calculation obtained with touching spheres.

While no appreciable preferences can be drawn from the observation of the overall agreement with the experiment of the ''geometries'' $p(2\times2)$ and $c(4\times2)$ reported in Fig. 2, only slightly different geometrical parameters can be observed for the minimized geometries of the first three planes of the Si(001) surface. In all the calculations no twisting of the dimer bond was taken into consideration. The model that was followed for the relaxation of the structure did not take into consideration any shift or twist of the atoms in the [110] direction, i.e., perpendicularly to the dimers bond. Only in

TABLE I. The atomic displacements from the ideal Si(001) surface positions (units of Å) for the three periodicities for which calculations have been optimized $p(2\times1)$, $p(2\times2)$, $c(4\times2)$ and for the mixed geometry $c(4\times2)+p(2\times2)$. The atomic coordinates of ideal Si(001) surface are labeled by indices (k,l,m), for an atomic position vector $\vec{R}=(k/2*\sqrt{2},l/2*\sqrt{2},m/4)*a$, where a is the lattice constant of bulk silicon. The x direction is along the crystallographic $[1\bar{1}0]$ direction and x is along $[110]$.

Atoms	$p(2\times1)$			$p(2\times2)$			$c(4\times2)$			$c(4\times2)+p(2\times2)$		
(k,l,m)	δx	δy	δz	δx	δy	δz	δx	δy	δz	δx	δy	δz
(0, 0, 0)	+0.66(2)		−0.04(2)	+0.59(2)		−0.09(2)	+0.60(2)		−0.10(2)	+0.63(2)		−0.05(2)
(2, 0, 0)	−1.04(4)		−0.50(2)	−1.02(4)		−0.72(2)	−1.10(4)		−0.82(2)	−1.03(4)		−0.76(2)
(0, 2, 0)	+0.66(2)		−0.04(2)	+1.02(4)		−0.72(2)	+1.10(4)		−0.82(2)	+1.03(4)		−0.76(2)
(2, 2, 0)	−1.04(4)		−0.50(2)	−0.59(2)		−0.09(2)	−0.60(2)		−0.10(2)	−0.63(2)		−0.05(2)
(0, 1,−1)	+0.10(2)		−0.07(2)	+0.10(2)	−0.07(2)	−0.07(2)	+0.10(2)	−0.05(2)	−0.10(2)	+0.10(2)	−0.05(2)	−0.07(2)
(2, 1,−1)	−0.10(2)		−0.07(2)	−0.10(2)	+0.07(2)	−0.07(2)	−0.10(2)	+0.05(2)	−0.10(2)	−0.10(2)	+0.05(2)	−0.07(2)
(4, 1,−1)	+0.10(2)		−0.07(2)	+0.10(2)	+0.07(2)	−0.07(2)	+0.10(2)	+0.05(2)	−0.10(2)	+0.10(2)	+0.05(2)	−0.07(2)
(6, 1,−1)	−0.10(2)		−0.07(2)	−0.10(2)	−0.07(2)	−0.07(2)	−0.10(2)	−0.05(2)	−0.10(2)	−0.10(2)	−0.05(2)	−0.07(2)
(1, 1,−2)			−0.15(4)			−0.20(4)			−0.15(4)			−0.15(4)
(3, 1,−2)			+0.05(2)			+0.05(2)			+0.05(2)			+0.05(2)
(5, 1,−2)			−0.15(4)			−0.20(4)			−0.15(4)			−0.15(4)
(7, 1,−2)			+0.05(2)			+0.05(2)			+0.05(2)			+0.05(2)

the case of $p(2\times2)$ and $c(4\times2)$ we allowed a relaxation of second-layer atoms in that direction.

The structural results obtained in this paper are summarized in Table I, respectively, for $p(2\times1)$, $p(2\times2)$, and $c(4\times2)$ and a mixed $[p(2\times2)+c(4\times2)]$ reconstructions. The resulting bond lengths and dimer tilt angles are depicted in the ball and stick model in Fig. 3. Looking at the values of the errors, one remarks that the sensitivity to the structure is isotropic and the technique does not suffer any lack of sensitivity in certain experimental conditions as could happen in some cases with x-ray surface diffraction, transmission electron diffraction, or x-ray standing waves.

In the case of the $p(2\times1)$ reconstruction the comparison with the experiment is not satisfactory ($R=0.08$), and this conclusion is confirmed by the geometrical parameters obtained for the reconstruction. Movements of the atoms in direction perpendicular to the dimer were not allowed. The value of the dimer angle was found to be $12°(\pm1°)$, while value of the bond length was equal to $2.18(\pm0.03)$ Å. This low dimer bond angle is in disagreement with the calculation of Dabrowski and Scheffler[17] (15°), the value found by Ramstad, Brocks, and Kelly[18] for the same reconstruction (18.3°) and that of Krüger and Pollmann[19] (19°). These values are quite different from the values reported in the earlier calculations[20–23] and ranging between 6° and 14° for the dimer bond angle. A lower value of the dimer bond angle for this reconstruction was reported in other experimental studies, often justified on the basis of the average of fast thermal vibrations of the dimer atoms. With the exception of ion-scattering measurements,[24] (14°), values ranging between 5° and 8° (Refs. 25–27) were observed.

The dimer bond length also shows a high degree of variation in the literature from 2.20 to 2.47 Å (Refs. 24–28) while theoretical calculations find a minimum in the total energy for values ranging from 2.22 to 2.29 Å.[17–23] The value of the backbond lengths with the second-layer atoms found in the present experiment, assuming a $p(2\times1)$ structure, are 2.44 and 2.33 Å, close to those found by Tromp *et al.* (2.43 and 2.37),[24] but larger than the value reported recently, i.e., 2.34 Å and 2.29 Å by Ramstad, Brocks, and Kelly *et al.*,[18] and 2.33 and 2.28 Å from Krüger and Pollman[19] and Zhu, Shima, and Tsukada.[21]

The $p(2\times2)$ reconstruction showed a sensitive increase in the dimer bond buckling $15.8°(\pm1°)$ and dimer bond length $2.31(\pm0.03)$ Å found by our experiment. The found backbond values were respectively 2.33 and 2.30 Å for the up and down atoms of the dimer. Very similar values of the dimer parameters were reported by Ramstad, Brocks, and Kelly[18] while the backbonds are respectively 2.34 and 2.31 Å. Tromp *et al.*[24] reported a value of the dimer length of 2.38 Å and a buckling angle of 15.5°. The determined backbonds values were respectively 2.37 and 2.16 Å. Shkrebtii *et al.*[29] reported for this reconstruction values of 18.4° and 2.38 Å, respectively for the dimer bond angle and length.

The $c(4\times2)$ reconstruction showed a dimer bond buckling comparable with that of $p(2\times2)$ with a buckling angle of $18.6°(\pm1°)$, dimer bond length of 2.26 Å, and backbond values of 2.36 and 2.30 Å, respectively, for the bond of the top and bottom atom of the dimer. The dimer geometries are in overall agreement with the result of the calculation of Northrup,[30] 17.7° and 2.29 Å for angle and length of the bond, and for the backbond lengths, respectively, 2.35 and 2.31 Å. Other calculations for this reconstruction were reported by Zhu, Shima, and Tsukada[21] who found an angle of 13°, a dimer bond length of 2.27 Å, and backbonds of 2.34 and 2.31 Å, respectively. In a recent work Ramstad, Brocks, and Kelly[18] found a value of the bond angle equal to 18.8° and bond length of 2.29 Å, with backbond values of 2.36 and 2.31 Å. Shkrebtii *et al.*[29] reported for this reconstruction a value of 16.9° and 2.38 Å, respectively, for dimer angle and length.

In order to show that the buckling angle is a sensitive parameter of the structure, a different minimization of the error between experiment and theory was done. The main

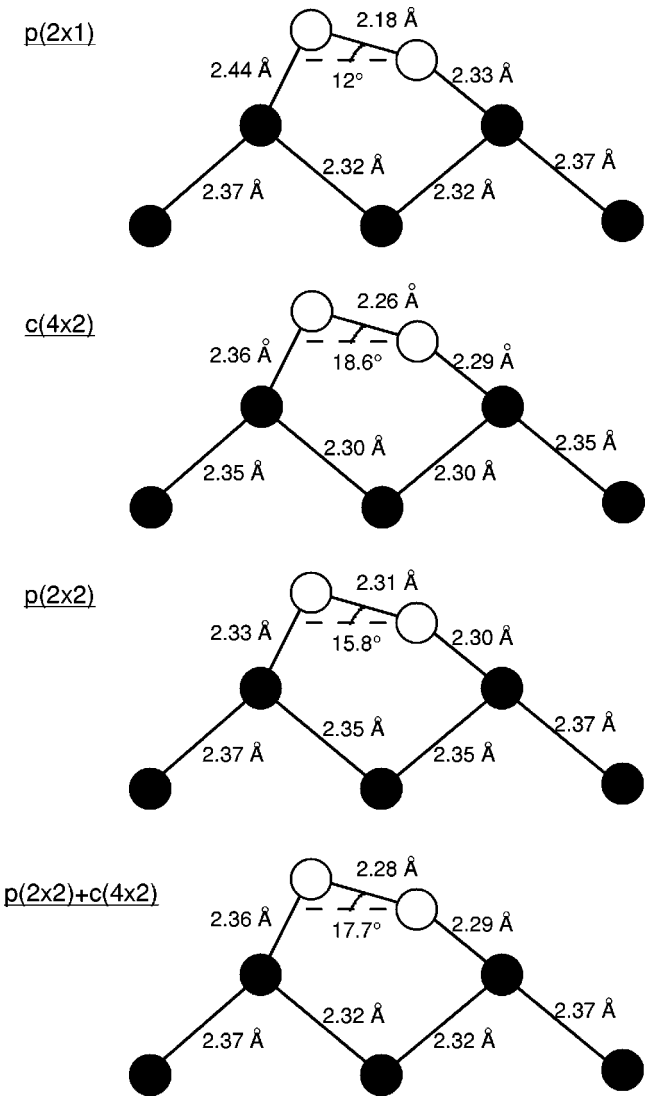

FIG. 3. Results of the geometrical optimizations for the bond lengths and angles of the dimer geometry sketched by stick and ball models for different surface periodicities (from top to bottom the $p(2\times1)$, $c(4\times2)$, $p(2\times2)$ and a mixed surface $[c(4\times2)+p(2\times2)]$.

task was to show that no local minima were present in the parameter space for different angles of buckling of the dimer. This procedure followed the following guideline: if some constraints are put to the bond length contraction and expansion (2%) only a few configurations will be available for the down atom of the dimer when the up atom is fixed. An *R*-factor plot for all these configurations for different up-atom positions as a function of the dimer angle can be well represented (in terms of the best agreement) by calculations done only at those configurations obtained by averaging the coordinate positions of the down atom. In this way we chose the surface configurations used in the plots of Fig. 4 with the above constraints of dimer bond and backbond length. These plots clearly show the sensitivity of the surface geometry to the dimer angle. In this case of the $c(4\times2)$ a minimum *R* factor resulted for a dimer length of 2.25 Å and backbond lengths of 2.34 and 2.33 Å at an angle of the dimer comparable with that of the more general minimization illustrated above.

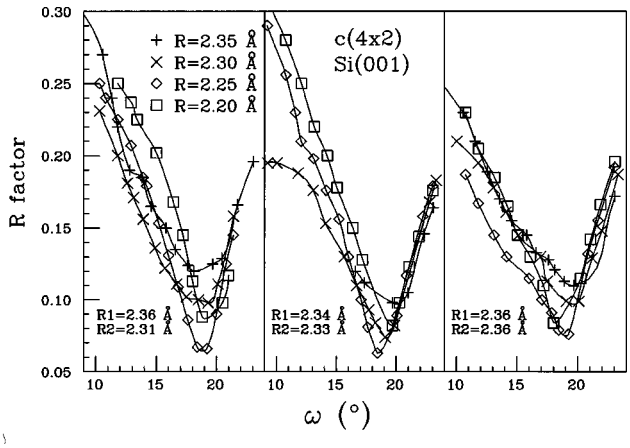

FIG. 4. Behavior of the *R*-factor plot of calculations of a $c(4\times2)$ reconstructed surface given three configurations of the backbond lengths ($R1=2.36$ Å, $R2=2.31$ Å; $R1=2.34$ Å, $R2=2.33$ Å; and $R1=2.36$ Å, $R2=2.36$ Å) and four values of the dimer length (2.35, 2.30, 2.25, and 2.20 Å) while varying the dimer angle in the way described in the text.

Similarly the same procedure applied to the case of the $p(2\times1)$ (not reported) led to the geometry of a slightly buckled dimer (about 11–12° degree) and a value of the dimer length of 2.30 Å.

In the above discussed approach the PD experiment was analyzed as if it were the product of an experimentally well characterized arrangement of dimers resulting in a single domain of reconstruction. This is probably quite far from the real surface derived from the disordered $c(4\times2)$ or $p(2\times2)$ surface. In principle the correct approach to the problem would involve a move from the single domain reconstructed surface arranging in an uncorrelated way the buckling direction of dimers. The same procedure was adopted in surface x-ray diffraction by Rossmann *et al.*[31] in the case of Ge(001)-2×1 surface and more recently by Felici *et al.*[32] for the Si(001)-2×1 surface. Even though in the case of a SCLS-PD analysis a smaller number of parameters are needed as only 3–4 planes are involved in the process, when compared with a number close to 7–10 in the case of surface x-ray diffraction, the application of the statistical model is difficult to accomplish here because it requires the realization of a large sample of surfaces with statistically switched dimers close to the position of the absorber up atom of the dimer. In an approximate way the effect of the disorder was simulated by looking at the theoretical signal coming from an equal occurrence of a $p(2\times2)$ and a $c(4\times2)$ reconstructions on the surface in order to look at the variations induced in the structural parameters. In this case of double domain surface the final result achieved a similar level of agreement with the experiment and a similar value of the *R* factor (0.052) to the case of the single reconstruction geometry. On the other hand the structural parameters found showed some differences with the single domain cases as reported in Table I for the mixed geometry. Corresponding values are reported in a stick and ball picture also in Fig. 3. The results were not far from those of the two single domain reconstructions $c(4\times2)$ and $p(2\times2)$, confirming in this way the overall stability of the present minimization procedure. The resulting values for the up and down dimer atoms backbond were

respectively 2.36($\pm$0.03) Å and 2.29($\pm$0.03) Å. The buckling angle was 17.7°($\pm$1) and the dimer length was 2.28 ($\pm$0.03) Å. This values are in excellent agreement with the theoretical work of Northrup.[30] When we compare the present result with the experimental results of Felici *et al.*[32] we observe in their geometry a substantially larger value of the buckling angle [20°($\pm$3)] and of the dimer length (2.67 Å).

IV. CONCLUSIONS

There is now general consensus on the ''antiferromagnetic'' arrangement of Si dimers on the 2×1-Si(001) even at room temperature. This observation finds the theoretical basis on the small differences between total energies of $p(2\times1)$, $c(2\times2)$, $p(2\times2)$, and $c(4\times2)$ reconstructions, which was demonstrated to be a consequence of electrostatic interactions between surface dimers.[33]

At least in regions where the buckling is not pinned by defects, we can represent the surface consisting of a dimer superstructure in which their constituent dimers flip at high frequency resulting in local arrangements of different reconstruction orders: $p(2\times1)$, $p(2\times2)$, and $c(4\times2)$. Their distribution should also depend on the sample preparation procedure and sample type. For example, as found by Landemark *et al.*[34] with a highly *n*-doped crystal, it was not possible to obtain a $c(4\times2)$ LEED pattern but only half order streaks upon cooling. A picture of Si(001) with a fundamental $c(4\times2)$ reconstruction in agreement with the work of Tabata *et al.*[4] was given by photoemission experiments[7,34] in which RT (2×1) LEED pattern surface showed a surface band structure with a second dangling bond that would not be compatible with the 2×1 periodicity. In particular the sample used in the present experiment was of the same kind as that used in the work of Enta and co-workers[7] showing a clear phase transition to the $c(4\times2)$ periodicity after cooling.

The aim of the present work is to present with theoretical detail a method based on a full multiple scattering with complex potential particularly efficient for calculation of SCLS-PD in the very low kinetic energy range (40 eV) of the electrons, where their sensitivity to the surface is the highest, and the tough problem of clean surfaces affordable. The application to the case of the RT partially disordered Si(001)-2×1 surface, though via a simplified approach to the statistical model, showed an excellent stability in the structural parameters found under the assumption of a surface consisting of a single domain or by an incoherent mixing of single domains of reconstruction, leading us to the conclusion that the technique is slightly sensitive to the partial configurational disorder.

The sensitivity to the geometry of clean surfaces of the present SCLS-PD technique, in the light of the present results, can be safely compared with that of other experimental techniques. Especially in the case of semiconductors, where some degree of disorder is expected on the surface, the shortness of the range probed by the technique is of great help for structure determination, avoiding the lack in accuracy that has been reported for techniques with the need for long-range order. Moreover the degree of sensitivity to geometrical parameters is isotropic, and a single experiment itself contains most of the information on such parameters.

In conclusion this paper brings to completeness a former study on the application of SCLS photoelectron diffraction to the clean 2×1-Si(001) surface.[2] In that previous work this versatile technique allowed us to discuss the structural assignment of SCLS peaks in the photoemission spectrum. In the present work the high sensitivity to the structural parameters and the stability of the solution found even in the present challenging case of rapidly switching buckled dimers on the surface is shown. The very short range nature of this technique makes it capable of giving reliable results on surfaces without long-range order.

ACKNOWLEDGEMENTS

This work benefited from computer resources due to the Consiglio Nazionale delle Ricerche (CNR) Research Contract No. 96.00844.ST76. This work was partly supported by the Swedish Natural Science Research Council.

*Present address: Experimentelle Physik I, Universität Dortmund, D-44221 Dortmund, Germany.

[1] S. Gota, R. Gunnella, Z. Y. Wu, G. Jézéquel, C. R. Natoli, D. Sébilleau, E. L. Bullock, F. Proix, C. Guillot, and A. Quémerais, Phys. Rev. Lett. **71**, 3387 (1993).

[2] E. L. Bullock, R. Gunnella, L. Patthey, T. Abukawa, S. Kono, C. R. Natoli, and L. S. O. Johansson, Phys. Rev. Lett. **74**, 2756 (1995).

[3] J. Ihm, D. H. Lee, J. D. Joannopoulos, and J. J. Xiong, Phys. Rev. Lett. **51**, 1872 (1983).

[4] T. Tabata, T. Aruga, and Y. Murata, Surf. Sci. **179**, L63 (1987).

[5] R. J. Hamers, R. M. Tromp, and J. E. Demuth, Phys. Rev. B **34**, 5343 (1986); R. Wiesendanger, D. Bürgler, G. Tarrach, and H.-J. Güntherodt, Surf. Sci. **232**, 1 (1990).

[6] R. A. Wolkow, Phys. Rev. Lett. **68**, 2636 (1992).

[7] F. J. Himpsel and E. E. Eastman, J. Vac. Sci. Technol. **16**, 1297 (1979); Y. Enta, S. Suzuki, and S. Kono, Phys. Rev. Lett. **65**, 2704 (1990); L. S. O. Johansson, R. I. G. Uhrberg, P. Martensson, and G. V. Hansson, Phys. Rev. B **42**, 1305 (1990).

[8] C. R. Natoli, M. Benfatto, C. Brouder, M. F. Ruiz Lopez, and D. L. Foulis, Phys. Rev. B **42**, 1944 (1990).

[9] R. Gunnella (unpublished).

[10] T. A. Tyson, K. O. Hodgson, C. R. Natoli, and M. Benfatto, Phys. Rev. B **46**, 5997 (1992).

[11] L. Hedin and S. Lundqvist, Solid State Phys. **23**, 1 (1969); J. Phys. C **3**, 73 (1972); **4**, 2347 (1971); **4**, 2064 (1971).

[12] E. Clementi and C. Roetti, At. Data Nucl. Data Tables **14**, 177 (1974).

[13] D. R. Penn, Phys. Rev. B **35**, 482 (1987).

[14] SCF Si-bulk charge density has been kindly provided by Professor S. Ossicini, University of Modena, Italy.

[15] R. Gunnella, E. L. Bullock, C. R. Natoli, R. I. G. Uhrberg, and L. S. O. Johansson, Surf. Sci. **352-354**, 332 (1996).

[16] W. H. Press, S. A. Teulosky, W. T. Wetterling, and B. P. Flannery, *Numerical Recipes* (Cambridge University Press, New York, 1992).

[17] J. Dabrowski and M. Scheffler, Appl. Surf. Sci. **56**, 15 (1992).

[18] A. Ramstad, G. Brocks, and P. J. Kelly, Phys. Rev. B **51**, 14 504 (1995).
[19] P. Krüger and J. Pollmann, Phys. Rev. B **47**, 1898 (1993); Phys. Rev. Lett. **74**, 1155 (1995).
[20] N. Roberts and R. J. Needs, Surf. Sci. **236**, 112 (1990).
[21] Z. Zhu, N. Shima, and M. Tsukada, Phys. Rev. B **40**, 11 868 (1989).
[22] K. Kobayashi, Y. Morikawa, K. Terakura, and S. Blügel, Phys. Rev. B **45**, 3469 (1992).
[23] M. T. Yin and H. L. Cohen, Phys. Rev. B **24**, 2303 (1981).
[24] R. M. Tromp, R. G. Smeenk, F. W. Saris, and D. J. Chadi, Surf. Sci. **133**, 137 (1983); for reviews, see G. V. Hansson and R. I. G. Uhrberg, Surf. Sci. Rep. **9**, 197 (1988).
[25] G. Jayaram, P. Xu, and L. D. Marks, Phys. Rev. Lett. **71**, 3489 (1993).
[26] N. Jedrecy, M. Sauvage-Simkin, R. Pinchaux, J. Massies, N. Greiser, and V. H. Etgens, Surf. Sci. **230**, 197 (1990).
[27] B. W. Holland, C. B. Duke, and A. Paton, Surf. Sci. **140**, L269 (1984).
[28] P. Soukiassian, L. Spiess, K. M. Schirm, P. S. Mangat, J. A. Kubby, S.-P. Tang, and A. J. Freeman, J. Vac. Sci. Technol. B **11**, 1431 (1993).
[29] A. I. Shkrebtii, R. Di Felice, C. M. Bertoni, and R. Del Sole, Phys. Rev. B **51**, 11 201 (1995).
[30] J. E. Northrup, Phys. Rev. B **47**, 10 032 (1993).
[31] R. Rossmann, H. L. Meyerhein, V. Jahns, J. Wever, W. Moritz, D. Wolf, D. Dornisch, and H. Schulz, Surf. Sci. **279**, 199 (1992).
[32] R. Felici, I. K. Robinson, C. Ottaviani, P. Imperatori, P. Eng, and P. Perfetti, Surf. Sci. **375**, 55 (1997).
[33] D. J. Chadi, Phys. Rev. Lett. **43**, 43 (1979).
[34] E. Landemark, C. J. Karlsson, Y.-C. Chao, and R. I. G. Uhrberg, Phys. Rev. Lett. **69**, 1588 (1992); E. Landemark, C. J. Karlsson, Y.-C. Chao, and R. I. G. Uhrberg, Surf. Sci. **287/288**, 529 (1993).